World Electric Vehicle Journal

MDPI

Article

Design, Production, and Verification of a Switched-Reluctance Wheel Hub Drive Train for Battery Electric Vehicles

Martin Vosswinkel [1,*], Andreas Lohner [1], Volkmar Platte [2] and Tobias Hirche [1]

[1] Cologne University of Applied Sciences, Campus Deutz, Faculty 07, Lab for electrical drives, Betzdorfer Str.2, 50679 Köln, Germany; andreas.lohner@th-koeln.de (A.L.); tobias.hirche@th-koeln.de (T.H.)

[2] ELEKTRISOLA Dr. Gerd Schildbach GmbH & CO. KG; Zur Steinagger 3, D-51580 Reichshof-Eckenhagen, Germany; v.platte@elektrisola.de

* Correspondence: martin.vosswinkel@th-koeln.de; Tel.: +49-221-8275-2092

Received: 11 October 2019; Accepted: 18 November 2019; Published: 21 November 2019

Abstract: This contribution deals with the topic of the consistent further development of a wheel hub motor for battery electric vehicles (BEV) based on the principle of an outer rotor switched reluctance machine (SRM). The research work presented in this paper was founded by the ERDF.NRW program, Investment for Growth and Employment and the European Regional Development Fund. The R&D project was named Switched-Reluctance fo(u)r wheel (SR4Wheel). Based on the experience made by first prototype Evolution 0 (EVO 0), developed in the Laboratory for Automation Engineering, Power Electronics and Electrical Drives of the Cologne University of Applied Sciences (CUAS), the test results of EVO 1, as well as the redesign, EVO 2 is presented in this paper. The prototype EVO 0, a first proof of concept leads to several optimizations and lessons learned for the predecessor model EVO 1. The overall target of developing such a gearless outer rotor wheel hub motor is the full integration of the complete machine including its power electronics into the given space between the original friction brake and the rim. Furthermore, due to the additional integration of the power electronics, great opportunities in terms of new vehicle design as well as retrofitting capabilities of already existing vehicle platforms can be achieved. Thereby, further drive train assembly space like the engine compartment is no longer necessary. The SRM does not require magnets for torque production which leads to independence from the changeable commodity prices on the rare earth element markets. This paper presents the developing process, testing, and verification of the innovative drive train concept starting with the final CAD of EVO 1. During the testing and verification process a machine characteristic mapping is performed on a drive train test bench and subsequently the results of a finite element analysis (FEA) are plausibility checked by the test bench results. The process continues with energy conversion test scenarios of the project demonstrator vehicle on a roller test bench focused on noise vibration harshness (NVH) behavior and efficiency. As a conclusion, the gained knowledge by evaluating two EVO 1 prototypes on the rear axle of the test vehicle, and the design for the front axle drive train EVO 2 will be presented. As a major task on the front axle, the limited space due to the large disc brake can be identified and solved.

Keywords: wheel hub motor; switched reluctance machine; BEV (battery electric vehicle); electric drive; EV (electric vehicle); finite element calculation; powertrain

1. Introduction

As the latest political and industrial discussions and decisions show, the reduction of CO_2 emissions are no longer a topic dedicated to the future but are here now. The current generation

living on our planet earth is the first one that can feel and see the implications of global warming, and at the same time it is the last generation that has the chance to counteract against the dangers.

The diesel affair impressively shows that even the biggest Original Equipment Manufacturers (OEMs) have to redefine their product platform and their powertrain family as well as their development philosophy faster than ever before.

Customer requirements such as economic efficiency, environmental sustainability, energy efficiency, and high driving ranges cannot be met by the current actual BEVs. New technologies and cost saving solutions have to be introduced to the market to satisfy customer needs in the future.

Research papers prove that the production of a battery electric vehicles (BEV) can produce as much CO_2 emissions as the production of internal combustion engine (ICE) vehicles including its first 80,000 km [1]. Therefore, simple mass production of BEVs will not be the key to counteract against global warming.

One of the highest ecological and economic problems of producing different kinds of BEV is the extraction of rare earth elements for the magnet production, which are essential for the most common electric motor used in BEVs: the permanently excited synchronous machine (PESM). More than 90% of this commodity is located in Asia which causes high economic dependency.

The switched reluctance machine (SRM) can help to overcome this problem since its rotor carries neither winding nor permanent magnets [2]. As an alternative to SRM machines and the need of rare earth elements, we need to mention synchronous reluctance motors with ferrit magnets. These machines make use of magnet material that does not rely on rare earth elements. Motors using this type of torque production are investigated in [3,4]. When comparing Syn-Reluctance motors to SRM's, the biggest advantage of SRM's is the complete lack of magnet material, and therefore a real simple and robust rotor, which can be produced and assembled very inexpensively, with no need for gluing parts or inserting magnets into the sheet material. This is the main reason why an SRM had been chosen as a wheel hub machine, as simple and price stable as possible for mass production in the future.

However, due to a high noise vibration harshness (NVH) problem and a complex control algorithm the SRM is still waiting for the breakthrough as an electric traction drive for passenger cars.

There are already certain good research papers available for the topic of in-wheel SRM as [5,6] shows, however none of them are able to present a complete running prototype vehicle with four in wheel SRM implemented inside the car. Furthermore, none of the presented machines managed to integrate the power-electronics into the machine and so far no SRM-in-wheel motor reached a high power-to-weight ratio, as Table 6 shows.

The dedicated goal of this research project is to overcome the disadvantages of the SRM to use it as a traction drive and additionally prove the possibility of an integration of the complete electric machine including power electronics into the given assembly space of a wheel. Thereby, great layout flexibilities for future BEVs are examined. Furthermore enhanced vehicle control algorithms like torque vectoring can be researched.

2. Machine Design Second Prototype (Evolution 1) and Construction

The analysis of the first SRM wheel hub drive train (WHDT) prototype Evolution 0 (EVO 0), presented in [7] provided a great deal of knowledge for the design process of the predecessor model EVO 1. The overall target of the integration of the WHDT into the given assembly space of a standard vehicle wheelhouse is being held successfully. This leads to the improved drive train design shown in Figure 1.

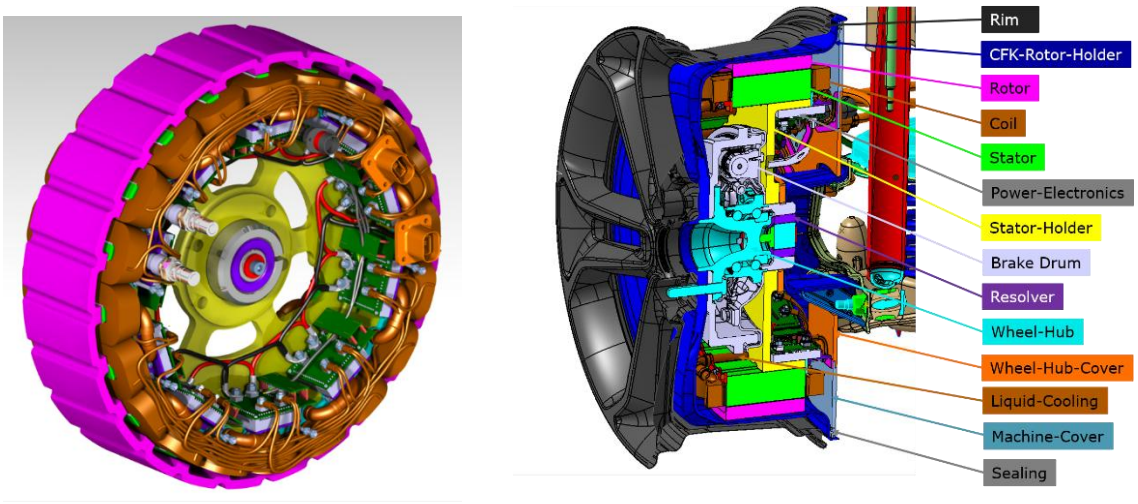

Figure 1. Mechanical concept of Evolution 1.

The high requirements to a WHDT such as high power density and mechanical robustness could be met by redesigning the power-electronics (grey), integrating a liquid cooling system (brown) and using a carbon fibre rotor holder (blue) with an integrated sealing system. The key values of EVO 1 can be obtained in Table 1.

Table 1. Key values of Evolution 1. Switched reluctance machine (SRM).

Parameter	Value	Unit
Type of machine	SRM	-
Number of phases	5	-
Number of stator teeth	20	-
Number of rotor teeth	24	-
Outer diameter	430	mm
Active length	100	mm
No. of turns per tooth	56	-
Air gap	1	mm
Torque at 0 rpm	520	Nm
Power at 1400 rpm	60	kW
Weight	<50	kg
Overall efficiency	>90	%

3. Production of Evolution 1

Two fully useable prototypes have been built up based on the design shown in Section 2 by using almost only internal resources of the Cologne University of Applied Sciences (CUAS) production possibilities. The achieved results can be seen in Figures 2 and 3.

Figure 2. Back and front Evolution 1 (EVO 1) plus integrated power electronics.

4. Test Bench Results and Finite Element Analysis Verification of Evolution

After performing several kinds of static and dynamic measurements with no load conditions, EVO 1 had been tested against a speed controlled Asynchronous Machine (ASM) to analyse and optimise each single working point (variation in speed and torque). A high speed measurement system (with 1 ms timestamp) including torque and speed measurements had been installed. In parallel, all voltage and current signals were logged with a precision power analyser to generate a view of EVO 1 machine characteristics with high resolution. While EVO 0 was only able to generate 25% of its maximum designed torque on the test bench through high radial deformation, the extreme stiff carbon fibre rotor of EVO 1 is able to show the full machine performance while maintaining the air gap of 1 mm. This leads into a starting torque of 523 Nm with a previous design goal of 520 Nm (refer to Table 1). In Figure 3, the basic overall efficiency of the whole wheel hub drive train including 10 power electronics modules (PEM) is shown:

overall Efficiency [%]																			
100	35.9	45.9	54.6	59.9	64.7	69.4	73.4	76.0	78.7										
90	38.3	48.9	56.7	62.9	67.3	71.2	74.3	76.8	79.9										
80	42.3	51.9	59.6	64.2	68.8	72.7	75.6	78.3	80.1										
70	45.3	54.8	61.4	67.1	71.3	74.3	77.7	78.9	80.5	82.2									
60	47.9	56.7	64.0	69.1	73.0	76.2	78.4	80.2	80.7	82.6	84.5	85.9							
50	51.1	59.9	66.9	71.4	74.6	78.0	78.4	81.3	80.7	82.4	84.2	85.8	86.6	86.5					
40	53.8	62.5	68.0	73.8	76.2	78.4	80.0	81.5	79.3	82.5	84.2	84.6	85.9	86.3	86.9	87.1	87.1		
30	54.8	62.4	68.8	73.8	77.2	77.2	78.3	80.3	80.5	82.1	84.7	84.4	85.0	85.4	86.1	86.3	86.5	85.8	84.9
20	55.3	61.6	67.1	72.1	73.9	77.2	76.5	80.6	78.9	78.0	81.4	80.9	82.6	83.1	82.6	82.9	83.6	83.5	84.3
10	49.9	56.1	59.8	64.1	72.1	72.9	72.7	75.0	76.6	75.3	76.6	76.8	79.1	78.5	77.3	78.7	78.5	79.7	79.3
Current [A] / Speed [rpm]	100	150	200	250	300	350	400	450	500	550	600	650	700	750	800	850	900	950	1000

Figure 3. Torque measurement vs. simulation comparison/Evolution 1.

Running only a basic machine mapping, the target of up to 90% efficiency (power electronics and SRM) could almost be achieved (maximum 87.1%). A more detailed efficiency analysis will be performed in Section 6.3.

Simultaneously to the efficiency analysis a comparison of simulated and measured torque was performed and shows satisfying results. By maintaining a difference between simulation and reality of <5% in almost all working points, the finite element analysis (FEA) simulation could be validated with great confidence. Figure 4 shows the machine torque versus speed curve for three different phase currents:

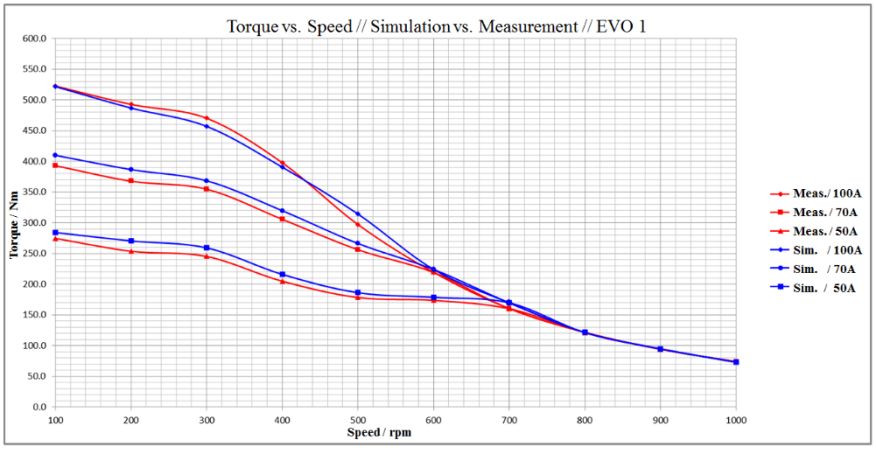

Figure 4. Torque measurement vs. simulation comparison/Evolution 1.

By validating the simulation with real measurements a powerful tool is now available to perform deep machine analysis based on simulations, before testing new parameters in the project demonstrator vehicle.

5. Installation in the Project Demonstrator and Testing of Evolution 1

After a successful validation on the test bench, the first two prototypes had been integrated into the project demonstrator vehicle. Showing the great capabilities of retrofitting this machine into the given vehicle, both machines had been integrated in less than 2 h. The result of the WHDT integration into the wheelhouse can be obtained in Figure 5.

Figure 5. Integrated EVO 1 in the project demonstrator.

To have maximum logging and control functions, a Controller Area Network (CAN) display with bidirectional communication had been installed inside the vehicle. With this interface, it is possible to record all machine data while performing tests on the roller test bench and on the street, shown in Figure 6. Thereby, it is possible to switch between different machine control settings, and this gives a comfortable opportunity to test different control algorithms while driving on the street without the need to reprogram the switched reluctance motor control unit (SRMCU).

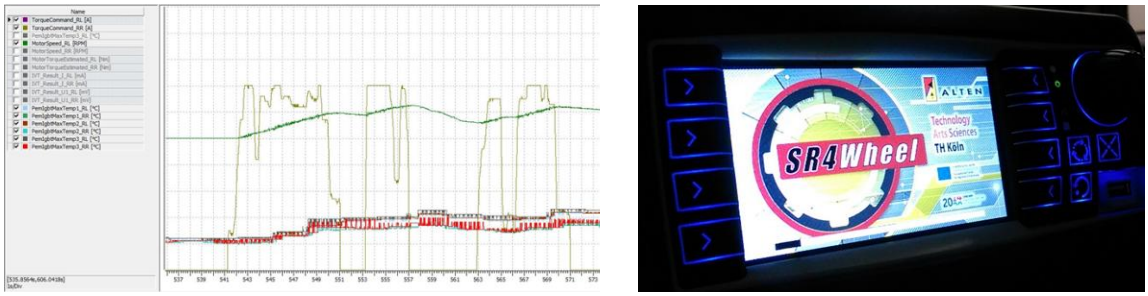

Figure 6. Recorded data during test drive and human machine.

After the successful high voltage and logical integration of both rear axle machines into the Ford Focus Electric test vehicle and a tested robust vehicle control unit behavior, the project demonstrator had been undergoing several different tests on the laboratory roller test bench, described in Section 6.

6. Driving Test Results

The main focus during all test scenarios on the roller test bench, as shown in Figure 7, was maximum reliability of the WHDT and repeatable behavior. Furthermore, two of the SRM natural disadvantages like the NVH behavior and efficiency were analysed and optimized in detail.

Figure 7. Project demonstrator on roller test bench.

6.1. Noise Vibration Harshness Optimisation

For a detailed view of EVO1 sound characteristics, audio recordings with wide frequency spectrum microphones had been performed. By transferring the recorded data by a fast Fourier transformation (FFT) into a frequency over time diagram, several different working points like low speed–high torque/high speed–low torque had been analysed. Two different frequency ranges could be identified:

1. Switching frequency in current hysteresis control (stable over complete machine operation),
2. Basic switching frequency of the five different phases (proportional to machine speed).

Furthermore it turned out that different basic switching frequencies are able to induce the harmonics of the resonance-frequencies of the carbon fibre rotor carrier and therefore higher vibrations inside these points could be obtained.

By reanalysing these working points at the simulation, a high torque ripple at exactly those points, due to the chosen switch-on, switch-off, so called "firing angle" points, could be identified.

The SRMCU controls the firing angle of each phase, based on the measured machine speed and the target hysteresis current control value e.g., at 400 rpm and 50 A current, Phase Switch On at 0.2 deg after unaligned and Phase Switch Off 1.5 deg before aligned position. These firing angle values are simulated previous testing via FEA, verified on the machine test bench, and stored via 2D-look-up tables at the control unit.

For improving the NVH characteristics, we developed a new firing angle machine mapping by trying to reduce the overall machine torque ripple inside the natural resonance-frequency points of the rotor carrier. By changing the switch-on switch-off angles, an optimal "handshake" in terms of torque transfer between the demagnetisation of the switch-off phase and the magnetisation of the switch-on phase could be realised. Figure 8 shows an example working point at 400 rpm, and 50 A, which proves that an ideal synergy of the different phase currents leads to minimum torque ripple while maintaining the torque amplitude. Note: Switching inside the current hysteresis control at 50 A is not shown in this diagram, to better point out the difference in torque shape without the torque ripple caused by the tolerance band width (same for Figure 13).

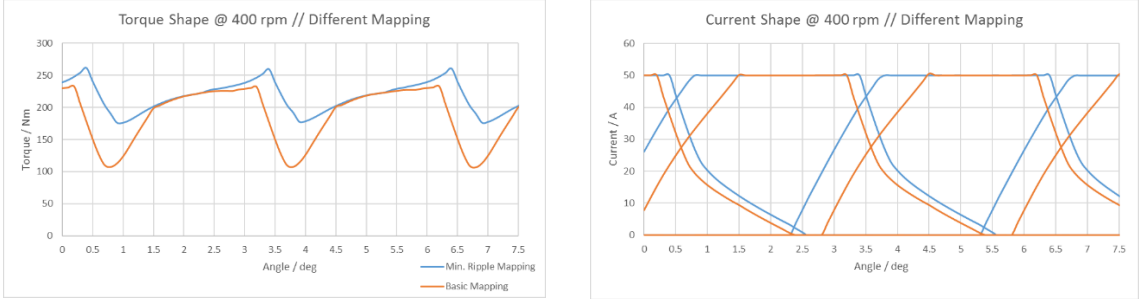

Figure 8. Different firing angles for minimum torque ripple.

By evaluating the optimum switching points for On/Off by the help of FEA calculations the torque ripple inside the shown example point has been significantly reduced.

Table 2 shows that the torque ripple had been reduced by >20% while the average produced torque gained 14% by changing the switch on point 0.5 deg and the switch off point 0.2 deg. The comparison between both acoustic measurements (basic versus minimum ripple map) at the example working point proves that by reducing the ripple, the noise behaviour of the machine can be improved.

Table 2. Parameter minimum torque ripple.

Parameter	Basic Map	Min. Ripple Map	Unit
Switch On Unaligned	0.5	0	deg
Switch Off Aligned	3.6	3.4	deg
Torque Ripple	54.2	32.6	%
Average Torque	191.4	219.4	Nm

Figure 9 shows the absolute sound pressure over the complete frequency range, in orange with high torque ripple, in blue with improved switching points. Easy noticeable is a reduction over the complete frequency range. Calculating the average noise amplitude for both measurements at the same working point shows that the noise amplitude of minimum ripple mapping is reduced by −3.2 dB, by parallel adding 14% torque. Using the described working process for the noise reduction of the machine, a new "NVH-friendly" machine mapping for all working points had been developed. These maps are stored in the SRMCU and can be controlled by the bidirectional CAN display inside the car.

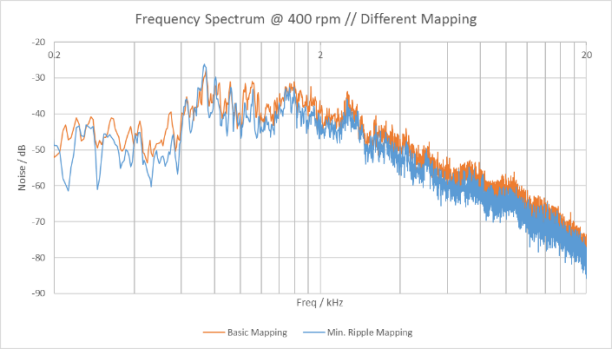

Figure 9. Frequency spectrum for two different machine maps.

6.2. Potential of Early Single Pulse Strategy (ESPS) for NVH Optimisation

A second possible solution to decerase the overall sound emissions of the SRM is a reduction of radial forces between the rotor and stator. A well known strategy to decrease these critial radial forces is to reduce the current amplitude inside a coil, linear to the overlapping between rotor and stator teeth. The more the teeth are aligned, the less current has to be drawn into the windings. To compensate the lack of torque, due to the low current at partial overlapping, a higher current amplitude at the unaligned position is drawn into the coil. Figure 10 illustrates the difference between the standard hysteresis current control (HCC) in grey and the early single pulse strategy (ESPS) in black as an example.

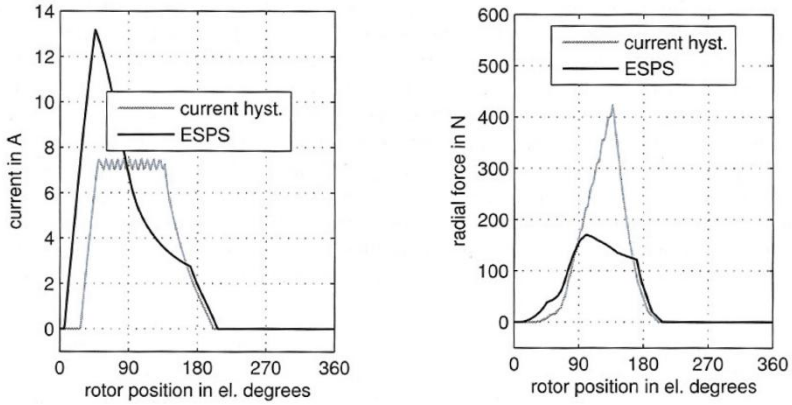

Figure 10. Example current waveforms at radial forces, hysteresis current control (HCC) vs. early single pulse strategy (ESPS) [8]. Reproduced from Knut, K., Analysis and Control of the Acoustic Behavior of Switched Reluctance Drives; published by RWTH Aachen, 2011.

Clearly noticeable is the lowered radial force by more than 50%. As a positive side effect, the acoustic influence of the switching frequency inside the current hysteresis control (refer to Section 6.1 Point No. 1) can be erased completely. Furthermore the efficiency of the power electronics can be increased by the lack of switching losses inside the HCC.

To test the acoustic influence of a single pulse control, this mode was implemented inside the PEM logic controller, and can be activated via the bi-directional display. When switching from HCC to single pulse, the upper border of the current control is increased by 20% to compensate for the lack of torque, while the switching on- and off-angles were kept identical. Figure 11 shows the available options inside the display and measured current waveforms inside one coil with a target current of 100 A.

Figure 11. Measured current waveforms HCC vs. single pulse/input via display.

After the successful implementation of this acoustic manipulation option inside all four machines of the project demonstrator test drives were made to measure the influence of the single pulse strategy to NVH behavior of the vehicle. To reach maximum objective results the measurements to fulfill the EU law regulation No. 540/2014 "Sound level of motor vehicles and of replacement silencing systems" was performed. To measure the sound pressure level of a vehicle several drives by tests (under constant speed and full acceleration) was performed. Figure 12 shows the measurement layout from the EU law as well as the practical test at the Aldenhoven proving ground close to Aachen.

Figure 12. Measurement layout [9] (Reproduced from Official Journal of the European Union; published by EU-Norm, 2014) and practical test at the Aldenhoven Proving Ground.

For getting a clear view about the influence of the single pulse, first the test vehicle was driven only by the front wheel drive (FWD) in HCC and single pulse, and afterwards both axles, all-wheel drive (AWD) in both current modes. Table 3 gives an overview over the reached sound pressure reduction.

Table 3. Measured sound pressure levels//HCC vs. single pulse.

Drive Mode	Current Control	Constant Speed	Full Acceleration	EU Calculated Value	Unit
FWD	HCC	85.3	92.2	88.8	dB(A)
		↓ −6.9	↓ −3.9	↓ −5.9	dB(A)
FWD	Single pulse	78.4	88.3	82.9	dB(A)
AWD	HCC	82.1	92.4	86.8	dB(A)
		−6	↓ −1.5	↓ −3.9	dB(A)
AWD	Single pulse	76.1	90.1	82.9	dB(A)

At maximum, −6.9 db (A) could be reached (at constant speed and FWD) which is more than a 50% sound pressure reduction. These first measurements were able to show the large influence of rotor radial forces to the NVH behavior of the designed SRM. In the future, a combination of minimum torque ripple control (as shown in Section 6.1) and radial force control via single pulse current waveforms (Section 6.2) will be investigated to reach further improvements at the NVH behavior of the designed SRM.

6.3. Efficiency Optimisation and New European Driving Cycle Test Results

After focusing on NVH behavior of the new WHDT, the machine efficiency improvement was identified as a second working package during test drives on the roller test bench. For a plausible comparability between the developed wheel hub drives automotive OEM drive trains, a fast-logging and high resolution current and voltage probe had been inserted on the output of the vehicle battery. Several New European Drive Cycles (NEDC's) cycles were performed with the original OEM drive train on the roller test bench to use the logged data as a reference. After installing the two new motors on the rear axle of the car and uninstalling of the original drivetrain these drive cycles had been repeated using the standard machine firing angle map. Due to the fact, that the measurement device and the test environment on the roller test bench had been identical, the results could be directly compared.

First results had been shown, that especially under partial load points (Target current <50 A) in the range of <400 rpm, the developed SRM has a poor efficiency. Please refer to the efficiency table in Figure 3 for a detailed look. These load points are very common inside the NEDC, whereby the targeted efficiency improvements were focused on this area. When requesting a certain specific drive torque to accelerate the vehicle, from machine mapping point of view, there are three degrees of

freedom: 1. Switch On Phase, 2. Switch Off Phase and 3. Current Amplitude. There are almost infinite combinations of these three parameters by producing the same requested torque at a given speed.

Using this freedom, the FEA calculation was used to identify the combination of the parameters for each partial load point. Figure 13 illustrates, that the same amount of torque can be produced by decreasing the time of current inside the coil but increasing the amplitude. To keep the example easy, only the copper losses are compared.

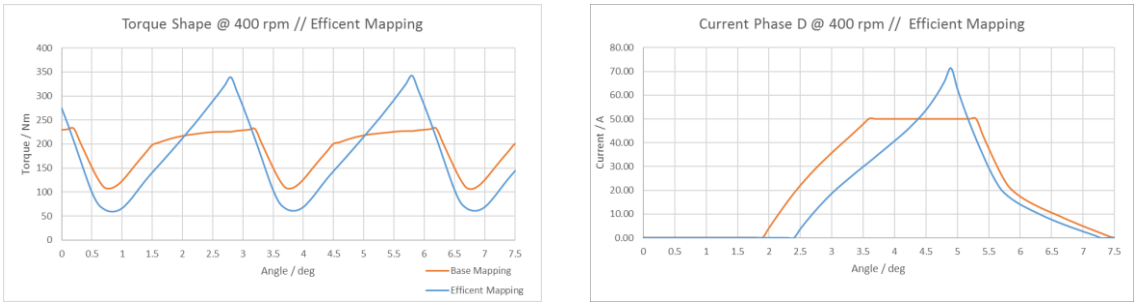

Figure 13. Different current shapes for identical torque.

Using the coil resistance and time of current inside the coil, the energy losses can be compared, as illustrated in Figure 14.

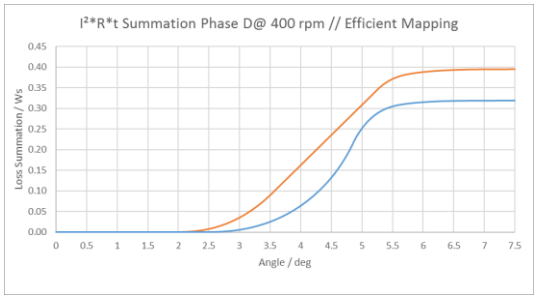

Figure 14. Energy loss comparison.

Considering the example point, the energy losses had been reduced by almost 20% by keeping the requested torque stable at 191 Nm, as it can be obtained in Table 4.

Table 4. Parameter maximum efficiency map.

Parameter	Basic Map	Max. Efficiency Map	Unit
Switch On Angle	0.5	1	deg
Switch Off Angle	3.6	4	deg
Current Amplitude	50	70	A
Average Torque	191.4	190.7	Nm
Energy Loss	0.395	0.319	Ws

On the other hand it is obvious that this efficiency gain has to be "paid" by an increased torque ripple from 54.2% in standard basic mapping to 82.4% in efficiency mode (remember 32.6% in NVH mode) which directly leads into a poor NVH behavior if running the efficiency map.

Depending on the operation point, e.g., the driver torque request, the best compromise between NVH, efficiency, and torque production has to be identified and implemented inside the machine mapping.

After proving that it is possible to maximise the efficiency of the WHDT, all working points had been optimized and stored at the SRMCU to be activated as "efficiency driving mode" via the display. Repeating the NEDC drive cycle the results can be analyzed in Figure 15: The new mapping marked in blue can be compared to the base mapping in yellow as well as with the original Ford Focus Electric

drivetrain in orange and the theoretical needed power of a 100% efficient drivetrain in green. The new mapping showed its capability for safe energy.

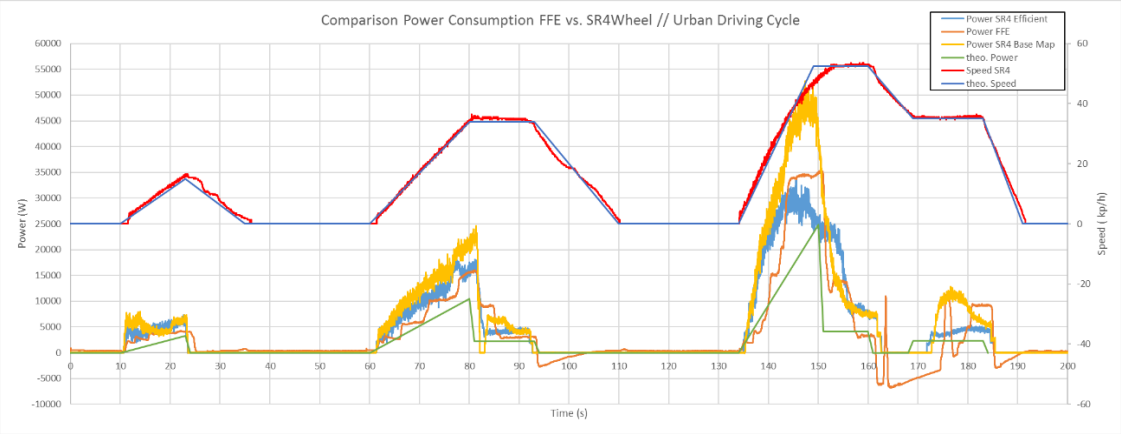

Figure 15. Test result: Original Ford vs. SR4Wheel rear axle vs. ideal power consumption.

While consuming more power during acceleration periods, the new SRM motor turned out to be more efficient during periods of constant speed. As a result in Table 5, the new motors are almost able to reach the energy consumption efficiency from the original OEM powertrain equipped with a single PESM driving the same NEDC profile.

Table 5. NEDC results.

Parameter	SR4Wheel	Ford Focus w/o Recuperation	Unit
NEDC Distance	9.91	10.3	km
Energy Consumption	2297.6	2313.5	Wh
Rated at 100 km	23.19	22.46	kWh/100 km
Rated Energy Consumption	103.2	100	%

These results are able to show, that a well suited and parametrised SRM is able to be competitive to a PESM in terms of overall efficiency under identical circumstances.

7. Machine Design Third Prototype Evolution 2

Simultaneously to the successful installation and testing of two EVO 1 machines on the rear axle, a final switched reluctance wheel hub motor for the front axle of the project demonstrator was developed. Keeping the overall goal of zero modification to the original vehicle including disc brakes, upright, and wishbones, the integration of a suitable machine turned out to be even more complex compared to EVO 1. Through the drum brake on the rear axle with a diameter of 270 mm and a 19 inch rim (diameter: 430 mm) EVO 1 had an radial installation space of 80 mm. Adapting this calculation to the front axle, EVO 2's integration is much more complicated. The size of the disc brake with a diameter of 334 mm let the radial installation space decreases to 48 mm, which is 60% of EVO 1. Furthermore, the moving parts at the front axle suspension like lower wishbone and steering link has to be taken into consideration when designing EVO 2. Due to the limited space, the power electronics of the front axle had to be outsourced into an extra housing. From an electro-magnetic point of view, the EVO 2 drive train adapts all lessons learned from EVO 1 and thereby leads into a design with 20 stator teeth, 24 rotor teeth, outer rotor: a five phased switched reluctance machine. Figure 16 shows flux and current density when phase D and E are energised as an example operating point.

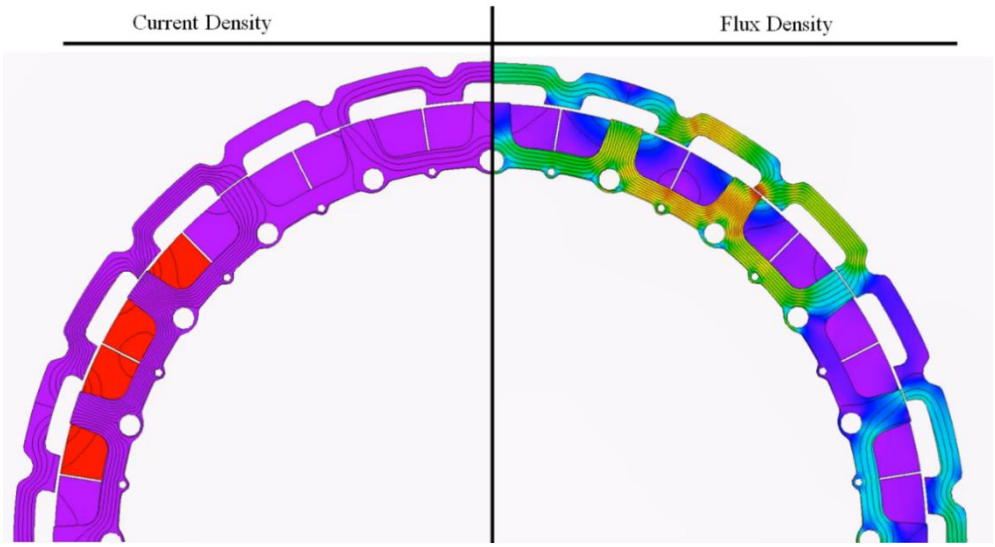

Figure 16. Flux and current density distribution EVO 2.

Due to the high current density the liquid cooling is placed even closer to the windings directly in the stator teeth compared to EVO 1, cf. Figure 1. The final Computer Aided Design (CAD) construction is shown in Figure 17.

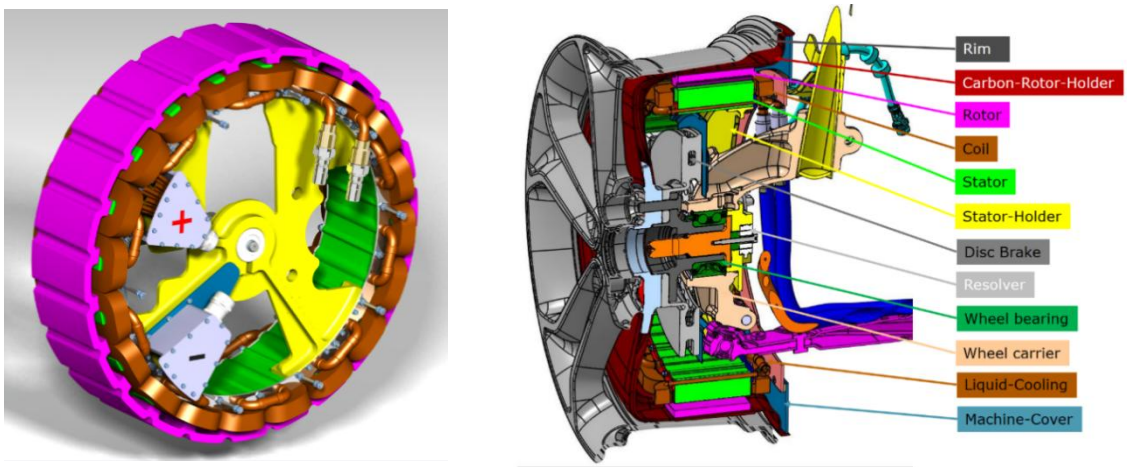

Figure 17. Mechanical concept of EVO 2.

Comparing EVO 2 to EVO 1, an additional 11 kg of machine mass could be saved, which leads to a weight reduction of 22%. The torque-speed characteristic of EVO 2 was designed to match perfectly the behaviour of EVO 1 on the rear axle: Producing less launch torque at lower speeds (due to the limited installation space) EVO 2 can produce more power at higher speeds to compensate for the rear axle which performs a power drop at >700 rpm. Overall the EVO 2 drive train is even 8% more powerful, at 22% less weight. Figure 18 shows the comparison of the front and rear machines over speed.

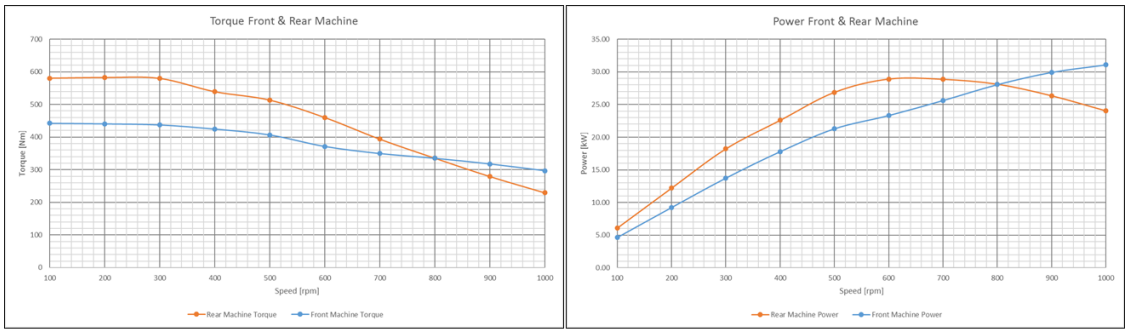

Figure 18. Torque and power for front and rear machines.

Thanks to the gained knowledge producing wheel hub SRMs, the manufacturing and assembly process of EVO 2 could be completed without problems. Figure 19 shows the complete, ready to install drive kit for the front axle. Clearly noticeable in the left Figure is the unaffected original disc brake inside the machine. The overall goal of integrating the machine into the given installation space on the front axle was achieved.

Figure 19. Back and front view of EVO 2.

8. Summary and Outlook

8.1. Summary

As shown in the previous chapters, the successor model of EVO 0, the model EVO 1 was successfully installed and tested at the project demonstrator vehicle. The EVO 1 drive train is able to produce >500 Nm launch torque, and reaches efficiency levels that are close to the original PESM with a 3.2% difference inside the NEDC. By developing the power electronics as well as the control unit, including its software, at the laboratory, a high degree of freedom for the machine controls can be reached cf. Section 6. By designing and manufacturing EVO 2 as a logical advancement of EVO 1 for the front axle, the project demonstrator can be equipped with four SRM wheel hub drives. The original drivetrain is removed and the complete empty space in the engine compartment of the car demonstrates the great flexibility of the new drivetrain in terms of vehicle platform concepts.

Even inside the prototype state of the machine and the power-electronics, it turned out that more expensive power electronics are not needed for the SRM, compared to a standard Permanent Magnet Synchronous Motors (PMSM). The used five semiconductor modules, containing a classical H-Bridge to drive all five phases of the machine were cheaper in sum, than a B6 bridge from the same manufacture at the identical voltage and current level. Due to the fact that the wheel hub motor is a low speed machine, windings can be connected in series to lower the total amount of current needed to drive one phase at nominal torque. Evo 1 produces its maximum torque of >500 Nm with a phase current of 100 A, comparing this to a classical PSM, a torque factor kt of 5 Nm/ARMS would be really

high. These facts show that the SRM is competitive to "classical" traction machines in terms of semiconductor costs.

The installed power and torque, using all four machines at a battery voltage level of 300 VDC can be identified in Figure 20.

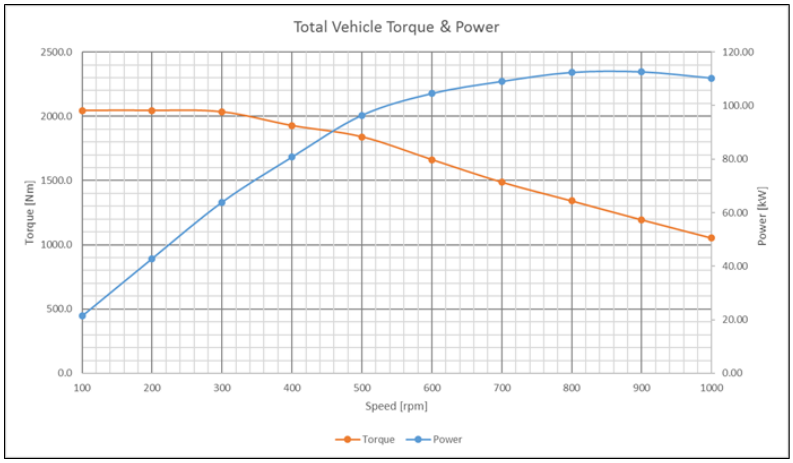

Figure 20. Full vehicle performance with four SRM.

A launch torque of >2000 Nm, and a constant power plateau of >100 kW at >600 rpm shows the good synergy effects between front and rear axle and leads into a vehicle acceleration performance of 8.6 s from 0–100 km/h. Table 6 summarises the most important key values of the three developed wheel hub motors.

Table 6. Final machine comparison.

Parameter	EVO 0	EVO 1	EVO 2	Unit
Number of Phases	2	5	5	-
Active Length	122	100	95	mm
Outer Diameter	430	430	430	mm
Air Gap	1.5	1	1	mm
Peak Torque at 100 rpm	169	523	442	Nm
Peak Power at 300VDC	5.8	28.1	31.8	kW
Peak Efficiency Drive Train-System	80.3	87.1	>90	%
Weight w/o Power Electronics	54.6	50.4	39.2	kg
Torque Density	3.1	10.4	11.3	Nm/kg
Power Density	0.11	0.56	0.81	kW/kg

Clearly noticeable is the gained knowledge about wheel hub SRM's during the design process from EVO 0 as a first proof of concept at the beginning of the project, designing a reliable five phase SRM with included power electronics for the rear axle EVO 1 with a power density of already 0.56 kW/kg, coming to the final machine EVO 2 for the front axle with a >40% higher power density of 0.81 kW/kg.

Notice: The potential of running the machines at 600 VDC, e.g., in other vehicles, would almost double their power.

On the other hand, adding almost 40 kg (in the case on EVO 2) of unsprung mass to the vehicle suspension may be judged critical for potential customers in the future. Due to the fact that both machines (EVO 1 and EVO 2) consist of a carbon-fiber-compound (CFK) rotor holder, with a lightweight optimized active rotor material, the weight of the rotating unsprung mass, which is even more critical, is only 11.5 kg. The variation inside standard usable rims on a passenger car (e.g., lightweight 17 inch rim versus heavy 19 inch rim) can already overcome this 11.5 kg, with no large noticeable effect on the driving behavior for a normal trained end-user of a vehicle.

In [10] Lotus Engineering proves that unsprung total masses (including suspension parts uprights etc.) from 50–80 kg are a problem that can be overcome by the adjustment of the suspension. "While perceptible differences emerge with increased unsprung mass, on the whole they are small and unlikely to be apparent to an average driver. The nature and magnitude of the changes appears to be nothing that cannot be overcome by the application of normal engineering processes within a product development cycle. Conversely, the promise of individual wheel motor control shows good potential for substantial improvements in vehicle behavior" [10].

8.2. Outlook

Both EVO 2 front axle machines will be installed and initially tested by the end of April 2019 inside the project demonstrator. Until the project SR4Wheel comes to its end in July 2019, several tests under real load conditions, such as maximum power test, reliability drives, and application of the specific developed dynamic vehicle control algorithms will be performed. Furthermore a bachelor thesis and master thesis, as well as a dissertation will take a deeper look into more advanced control algorithms for better NVH behaviour and efficiency as well as better torque density even after the finishing point of the official project.

Author Contributions: Investigation, M.V.; Project administration, A.L.; Software, V.P. and T.H.

Funding: This research was funded by the ERDF.NRW program, Investment for Growth and Employment and the European Regional Development Fund, grant number EFRE-0800348.

Conflicts of Interest: The authors declare no conflict of interest.

References

1. Romare, M.; Dahllöf, L. *The Life Cycle Energy Consumption an Greenhouse Gas Emissions from Lithium-Ion Batteries*; IVL Swedish Environmental Research Institute: Stockholm, Sweden, 2017.
2. Miller, T.J.E. *Switched Reluctance Motors and Their Control*; Oxford Science Publications: London, UK, 1993; ISBN 978-0-19-859387-4.
3. Omaç1, Z.; Polat, M.; Öksüztepe, E.; Yıldırım, M.; Yakut, O.; Eren, H.; Kaya, M.; Kürüm, H. *Design, Analysis, and Control of in-Wheel Switched Reluctance Motor for Electric Vehicles*; Springer: Berlin/Heidelberg, Germany, 2017.
4. Cinar, M.A.; Kuyumcu, F.E. Design and Torque Profile Analysis of an Outer-rotor SR Motor with Different Winding Configurations. *Prz. Elektrotech.* **2012**, *2*,328–331.
5. Kazuhiro, S.; Ryota, H. Shoji, S. Improved Ferrite Magnet Vernier Machine for an In-wheel Machine, In Proceedings of the 2012 IEEE International Conference on Power and Energy (PECon), Kota Kinabalu Sabah, Malaysia, 2–5 December 2012.
6. Bonthu, S.S.R.; Islam, M.Z.; Choi, S. *Design of a Rare Earth Free External Rotor Permanent Magnet Assisted Synchornous Reluctance Motor*; IEEE: Miami, FL, USA, 2017.
7. Vosswinkel, M.; Lohner, A. Design of a gearless wheel hub motor for BEV based on a switched reluctance machine. In Proceedings of the EVS30, Stuttgart, Germany, 9–11 Ocotober 2017.
8. Knut, K. *Analysis and Control of the Acoustic Behavior of Switched Reluctance Drives*; Shaker Verlag: Aachen, Germany, 2011.
9. European Union. Regulation (EU) No 540/2014 of the European Parliament and of the Council of 16 April 2014 on the Sound Level of Motor Vehicles and of Replacement Silencing Systems, and Amending Directive 2007/46/EC and Repealing Directive 70/157/EEC Text with EEA Relevance. 2014. Available online: https://www.eumonitor.eu/9353000/1/j9vvik7m1c3gyxp/vjs5ga5n1syz (accessed on 29 May 2019).
10. Martyn, A.; Damian, H. Unsprung Mass with In-Wheel Motors—Myths and Realities. In Proceedings of the *AVEC'10,* Loughborough, UK, 22–26 August *2010*.